

# Simulated Programmable Apertures with Lytro

Yangyang Yu  
Stanford University  
yyu10@stanford.edu

## Abstract

*This paper presents a simulation method using the commercial light field camera Lytro, which allows simulation of various aperture shapes and noise characteristics. A modified shift-and-add algorithm is used to implement aperture shape simulation. Two example use cases, special bokeh effects generation and multiplexed light field acquisition analysis, are given to demonstrate the system. Comparing to the conventional approaches, the proposed simulation system provides both convenience and flexibility.*

## 1. Introduction

In recent years, many researches are conducted in coded apertures for various applications including refocusing [14], deblurring [16], denoising [8] and depth of field estimation [6].

To demonstrate the effect of a certain coded aperture, usually a camera system with modified or programmable aperture is built for the purpose [8] [10]. However, the recent development in light field cameras might have provided a new option for us. With the consumer light field camera Lytro [11], we are able to capture an array of images of the same scene, from which we can effectively simulate apertures of various shapes. As a result, we would no longer need to build complicated system for each aperture. Instead, we could generate the simulated results through image computation. Such method provides great convenience in studying the effects of specific aperture shapes.

In this paper, two example use cases are presented. First, we designed a post-capture procedure to generate various out-of-focus blur, also known as bokeh, effects. Second, we studied a multiplexed light field acquisition method reported by Liang et al.[8].

## 2. Related Work

### 2.1. Camera Simulation

For decades, people have been working on camera models for simulation purpose[4] [9] [12]. However, most sys-

tems focus on rendering images from a synthesized 3D model. The simulation system reported in this paper allows users to capture real life scenes as the simulation base contents.

### 2.2. Special Bokeh Effects

It is a common technique for photographers to utilize the out-of-focus blur to add aesthetic value to their work. Many researches seek for methods to manipulate the out-of-focus blurs after an image is captured, in order to provide more post-processing options for photographers.

Lanman et al. reported a post-capture method for full-resolution control of the shape of out-of-focus points[5]. However, the available bokeh shapes are limited by a pre-selected training set. The paper reported a set of 12 different shapes.

Wu et al. developed a mathematical model for bokeh effects due to lens stop and aberrations to be able to render realistic out-of-focus blurs for synthesized image[15]. They did not explore the effects of various aperture shapes specifically.

Kodama et al. developed an algorithm to render deformed bokeh shape from multiple differently focused images by restoring light field images from differently focused images[3]. The paper reported results on simulated focal stacks. The authors reported planned future work to improve the robustness of the algorithm and extend the method to real images.

### 2.3. Multiplexed Light Field Acquisition Analysis

To demonstrate the potential of our simulation system in the research field, we chose a coded aperture related research, 'Programmable Aperture Photography: Multiplexed Light Field Acquisition' by Liang et al. We compared the research method reported by [8] and the simulation method presented in this paper.

More specifically, [8] presented a light field acquisition method using multiplexed images. The goal is to acquire a 3x3 light field. They capture nine images with a set of nine pre-computed multiplexing aperture patterns. Then,

a demultiplexing operation is used to reconstruct the light field images  $\mathbf{I}_{\text{LightFields}}$ .

The multiplexing patterns can be represented by a  $9 \times 9$  matrix  $\mathbf{W}$ , where each row of  $\mathbf{W}$  is a multiplexing pattern. The multiplexing image capture process can be represented by

$$\mathbf{I}_{\text{Samples}} = \mathbf{W} \cdot \mathbf{I}_{\text{LightFields}}.$$

The demultiplexing operation for reconstructing the light field images is therefore

$$\mathbf{I}_{\text{LightFields}} = \mathbf{W}^{-1} \cdot \mathbf{I}_{\text{Samples}}.$$

The multiplexing patterns are physically implemented with modified camera lenses where the aperture is masked with a set of paper scroll masks or a programmable LCD panel. The capture process is physically performed by taking the sample images in sequence. The demultiplexing process is performed through computation.

The paper reported higher image quality by using the multiplexed light field acquisition method. The reconstructed images are reported to show less noise than the light field images directly captured through pin holes.

However, the reported results are generated by the specific Nikon camera used in the research, which imposes a unique noise characteristic. We would like to further analyze the multiplexed light field acquisition method under a more flexible controlled environment with our simulation system.

### 3. Algorithms and Implementations

In this section, we first describe the fundamental algorithms and implementations to simulate various aperture shapes with light fields captured by Lytro. Then, more detailed algorithms and implementations for each of the examples are presented.

#### 3.1. Aperture Shape Simulation with Lytro

The commercially available light field camera Lytro Illum captures a 4D light field consists of  $14 \times 14$  views. Each of the views corresponds to the image captured through a portion of the aperture[1]. The shift-and-add refocus algorithm reported by Ng is used to synthesize a 2D image from the 4D light field. The mathematical representation is cited below. Details of the representations can be found in [11].

$$E_{\alpha,F}(x',y') = \frac{1}{\alpha^2 F^2} \int \int L_F^{(u,v)}(u(1-1/\alpha) + x'/\alpha, v(1-1/\alpha) + y'/\alpha) dudv$$

Notice that this algorithm integrates over all available sub-aperture images to synthesize the image that would be captured with a fully opened aperture. In this paper, we modify

the algorithm to integrate over a selected set of sub-aperture images to generate results with a specifically shaped aperture. The modified algorithm is given below.

$$E_{\alpha,F}(x',y') = \frac{1}{\alpha^2 F^2} \int \int M(u,v) L_F^{(u,v)}(u(1-1/\alpha) + x'/\alpha, v(1-1/\alpha) + y'/\alpha) dudv$$

$M$  is a matrix that defines the desired aperture shape. It is obvious from the equation that  $M$  imposes a weight on each of the sub-aperture images. Thus the synthesized result will show the effect of adding a mask onto the aperture. The value of  $M(u,v)$  indicates the ratio of light allowed to pass through the aperture location  $(u,v)$ . A value of 1 indicates a complete opening; A value of 0 indicates a complete block. When  $M$  is binary, the mask indicates an aperture opening shape. In the two examples, we will be working with binary masks. But the system is capable of simulating more complicated masks.

#### 3.2. Special Bokeh Effects

Two special bokeh effects were simulated, shaped bokeh and swirly bokeh.

##### 3.2.1 Shaped Bokeh

Bokeh shapes are mainly determined by the shape of the aperture. With conventional camera, photographers can also change the bokeh shapes by covering the lens by a mask with special shaped opening. The process can be easily simulated by the modified add-and-shift method described in 3.1. Figure 1 shows an example  $M$  that can be used to generate heart shaped bokeh.



Figure 1. A heart shaped mask.

##### 3.2.2 Swirly Bokeh

Some vintage camera lenses have the ability to create swirly bokeh due to their lens distortion. An example is given in Figure 2.



Figure 2. An example of swirly bokeh[2].

As we can see, the bokeh in the background are in various directions. They are arranged in a circular pattern. This effect is hard to achieve by simply applying a mask over a regular camera lens. But due to the flexibility of our computational process, we can simulate it by applying the mask at different directions at different pixel locations. To generate a centrosymmetrical arrangement as in the example, we transform the mask matrix  $M$  at each pixel location based on the location's angular coordinate.

$$M'(u, v, x', y') = H(M(u, v), \arctan(\frac{y' - h/2}{x' - w/2}))$$

$M'$  denotes the transformed mask.  $H$  denotes the transformation function. The function detail determines the final bokeh effects.  $h$  denotes the height of the 2D sub-aperture images.  $w$  denotes the width of the 2D sub-aperture images. The transformed mask  $M'$  is then applied during the shift-and-add process.

$$E_{\alpha, F}(x', y') = \frac{1}{\alpha^2 F^2} \int \int M'(u, v, x', y') L_F^{(u, v)}(u(1 - 1/\alpha) + x'/\alpha, v(1 - 1/\alpha) + y'/\alpha) dudv$$

### 3.3. Multiplexed Light Field Acquisition

Figure 3 shows the procedure of generating one simulated sample for the light field acquisition research. First,  $3 \times 3$  views are select from the Lytro captured  $14 \times 14$  light field views to match the light field specifications of the referenced research. We chose a well-lit scene and a set of well-exposed light field images, so that the set of images can be considered as the gold reference. Next, the masked shift-and-add algorithm described in section 3.1 is applied using the multiplexed pattern as the mask to synthesize the multiplexed image. These two steps can simulate the images captured under ideal situation with no noise presented. To better simulate the image capturing process and to target the research goal, simulated noise is added onto the samples. Figure 4 shows nine simulated multiplexed image samples.

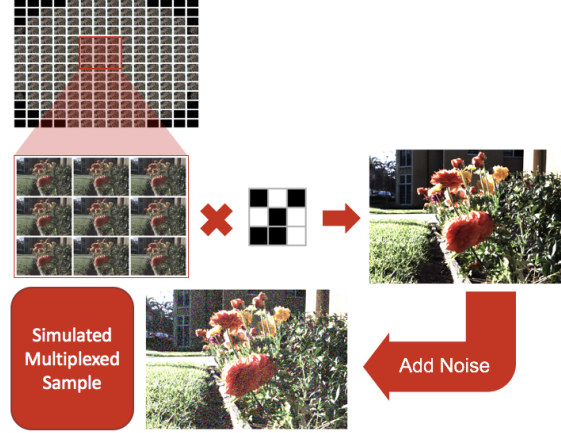


Figure 3. Summary of the light field acquisition simulation algorithm.



Figure 4. Simulated multiplexed images.

It is worth noticing that we can use the same procedure to simulate the light field images with straightforward acquisition. The mask will have one single opening in this case. Figure 5 shows nine simulated straightforward acquisition samples.



Figure 5. Simulated straightforward acquisition.

We then apply the demultiplexing algorithm described in

section 2.3 to reconstruct the light field images as shown in Figure 6.

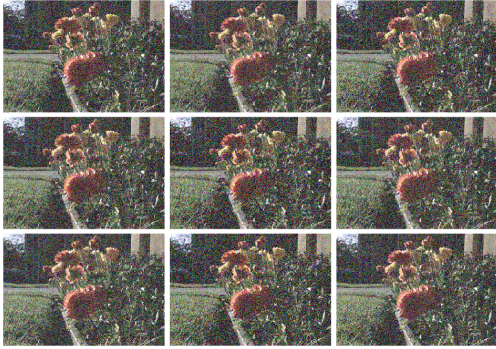


Figure 6. Light field images reconstructed from simulated multiplexed samples.

## 4. Results and Analysis

### 4.1. Special Bokeh Effects

#### 4.1.1 Shaped Bokeh

Table 1 gives some images with simulated shaped bokeh. The masks used to generate the images are also presented.

Table 1. Shaped Bokeh Results

Mask	Image

#### 4.1.2 Swirly Bokeh

We chose an ellipse shaped mask  $M$  as the pre-transformation mask, as shown in Figure 7.

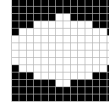


Figure 7. An ellipse shaped mask.

Table 2 are some images with simulated swirly bokeh. The corresponding transformation function  $H$  of each image is also presented. The first image is a reference image generated by the direct shift-and-add algorithm with no mask or transformation applied.

Table 2. Swirly Bokeh Results

Transformation Function	Image
$N \setminus A$	
$flip(imrotate(M, \theta))$	
$imrotate(M, \theta)$	
$transpose(imrotate(M, \theta))$	

$\theta = \arctan(\frac{y'-h/2}{x'-w/2})$ .  $imrotate(M, \theta)$  rotates the mask  $M$  counterclockwise around its center point by  $\theta$  while keeping the same matrix dimension.  $flip$  flips the matrix vertically.  $transpose$  takes the transpose of the matrix.

#### 4.1.3 Analysis

As we can see, the synthesized results look interesting and realistic. It is very ideal for visual and artistic purpose. We

can apply any arbitrary mask with a resolution of  $14 \times 14$ . The process is significantly simplified comparing to the conventional method of creating physical masks. Additionally, the flexibility of applying different masks at different locations gives the users more freedom in generating creative images.

## 4.2. Multiplexed Light Field Acquisition

### 4.2.1 Multiplexing Patterns Reported by [8]

As mentioned in section 3.3, the simulation system allows us to add simulated noise, which gives us the opportunity to further analyze the multiplexed acquisition algorithm reported by Liang et al [8]. We analyzed Gaussian and Poisson noise distribution individually, since they are the most common noise distribution in digital imaging. The results are given in visual forms in Figure 8 and Figure 9. The results are also compared with gold reference and the mean squared error are computed as a measurement for noise. The plots are given in Figure 10.

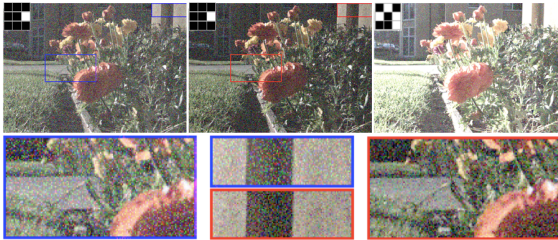


Figure 8. Straightforward Acquisition vs. Multiplexed Acquisition assuming only Gaussian noise. First row from left to right: simulated straightforward acquisition image, light field image reconstructed from simulated multiplexed samples, and simulated multiplexed acquisition image. Second row: Close-ups of the straightforward acquisition image and the reconstructed light field image.

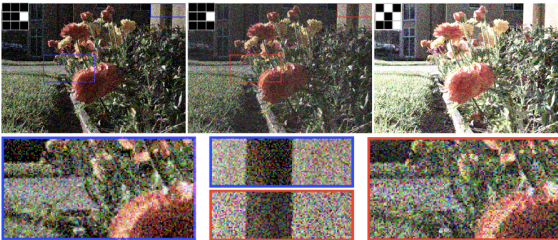


Figure 9. Straightforward Acquisition vs. Multiplexed Acquisition assuming only Poisson noise. First row from left to right: simulated straightforward acquisition image, light field image reconstructed from simulated multiplexed samples, and simulated multiplexed acquisition image. Second row: Close-ups of the straightforward acquisition image and the demultiplexed light field image.

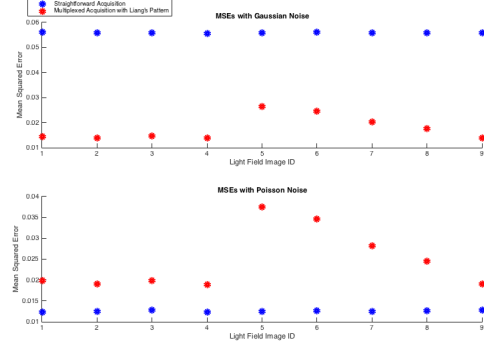


Figure 10. Mean square errors of the straightforward acquisition images and the demultiplexed light field images comparing to gold reference. The blue data points correspond to straightforward acquisition images while the red data points correspond to demultiplexed light field images. The top sub-plot is with Gaussian noise only and the bottom sub-plot is with Poisson noise only.

As we can see from both the visual results and the mean squared error measurement, the multiplexing algorithm reduced Gaussian noise but increased Poisson noise, which shows that the algorithm does not reduce all types of noise. We can further deduce that Liang et al. reported decrease in noise due to the specific camera's noise characteristic. It is most likely dominated by Gaussian noise.

Since we showed that the multiplexing algorithm's performance varies among different cameras, it will be both helpful and necessary to simulate the process with our simulation system and verify the performance of the algorithm before applying the algorithm to other devices.

### 4.2.2 Alternative Multiplexing Patterns

Another advantage our simulation system provides is the convenience to simulate various aperture patterns. In this use case, it gives us the opportunity to simulate and analyze an alternative set of multiplexing patterns.

#### Pattern Generation

According to Liang [7], the mean square error of the demultiplexed signal is proportional to a function  $E(\mathbf{W})$ :

$$E(\mathbf{W}) = \text{Trace}((\mathbf{W}^T \mathbf{W})^{-1}),$$

where  $\mathbf{W}$  is the set of multiplexing patterns. The pattern generation process is thus an optimization process of finding a matrix  $\mathbf{W}^*$  that minimize  $E(\mathbf{W})$ . The optimization problem is solved by a projected gradient method reported by Ratner and Schechner[13]. The result generated by the projected gradient method is a matrix with elements range from 0 to 1. The sum of each row is limited by a parameter  $C$ . In our case, we limited  $C$  to 5. To generate a binary

mask from the result matrix, we used a threshold of 0.5. It is worth noticing that the method is non-deterministic. The result can vary due to random initial values. Thus we ran the optimization process multiple times and took the  $\mathbf{W}$  that gives the lowest  $E(\mathbf{W})$ . The multiplexing pattern  $\mathbf{W}$  we found is given in Figure 11

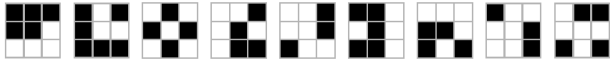


Figure 11. Alternative multiplexing patterns.

The performance of this multiplexing pattern is also measured by the mean squared error of the demultiplexed light field images comparing with the gold reference. The results are plotted in Figure 12

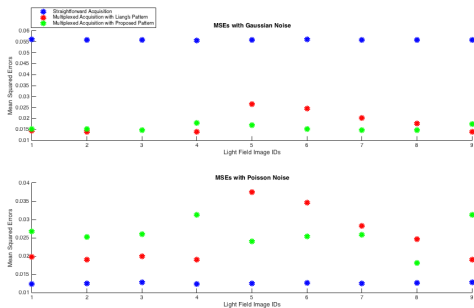


Figure 12. Mean square errors of the straightforward acquisition images, the demultiplexed light field images with the reference multiplexing pattern, and the demultiplexed light field images with the alternative multiplexing pattern. The blue data points correspond to straightforward acquisition images; The red data points correspond to demultiplexed light field images with the reference multiplexing pattern; The green data points correspond to the alternative multiplexing pattern. The top sub-plot is with Gaussian noise only and the bottom sub-plot is with Poisson noise only.

Similar to the reference multiplexing patterns reported by Liang et al., the alternative patterns reduce Gaussian noise but increases Poisson noise. Comparing the two sets of patterns, the alternative patterns has a lower average mean squared error in the Gaussian noise case and a higher average mean squared error in the Poisson noise case. However, the light field image 5 generated by using the reference patterns always results in the highest mean squared error in both cases. In many use cases, the quality of the light field can be limited by the worst light field view. The alternative pattern we found could be a better option.

Further researches using more sophisticated optimization algorithms could generate even more suitable multiplexing patterns. Here we demonstrated that our system provides a fast and convenient method to evaluate the generated patterns.

## 5. Conclusion

In this paper, we presented an aperture simulation system based on Lytro. We are able to demonstrate the advantage of the system through two use cases. We developed a special bokeh effect generation algorithm and further analyzed a multiplexed light field acquisition algorithm. Comparing to the existing methods, our system simplifies the result generation procedure, reduces the development effort, and provides more control over the environment.

## References

- [1] Lytro home, accessed March 12, 2016.
- [2] P. Hagger. The perfection in imperfection - kmz russian helios 40-2 85mm f1.5 lens, accessed March 12, 2016.
- [3] K. Kodama, I. Izawa, and A. Kubota. Robust reconstruction of arbitrarily deformed bokeh from ordinary multiple differently focused images. In *Image Processing (ICIP), 2010 17th IEEE International Conference on*, pages 3989–3992, Sept 2010.
- [4] C. Kolb, D. Mitchell, and P. Hanrahan. A realistic camera model for computer graphics. In *Proceedings of the 22Nd Annual Conference on Computer Graphics and Interactive Techniques, SIGGRAPH '95*, pages 317–324, New York, NY, USA, 1995. ACM.
- [5] D. Lanman, R. Raskar, and G. Taubin. Modeling and synthesis of aperture effects in cameras. 2008.
- [6] A. Levin, R. Fergus, F. Durand, and W. T. Freeman. Image and depth from a conventional camera with a coded aperture. In *ACM SIGGRAPH 2007 Papers, SIGGRAPH '07*, New York, NY, USA, 2007. ACM.
- [7] C.-K. Liang. *Analysis, Acquisition, and Processing of Light Field for Computational Photography*. PhD thesis, National Taiwan University, Taipei, Taiwan, R.O.C., June 2009.
- [8] C.-K. Liang, T.-H. Lin, B.-Y. Wong, C. Liu, and H. H. Chen. Programmable aperture photography: Multiplexed light field acquisition. *ACM Trans. Graph.*, 27(3):55:1–55:10, Aug. 2008.
- [9] A. A. Modla. Photographic camera simulation systems working from computer memory, Mar. 15 1988. US Patent 4,731,864.
- [10] H. Nagahara, C. Zhou, T. Watanabe, H. Ishiguro, and S. K. Nayar. Programmable aperture camera using lcos. In *Proceedings of the 11th European Conference on Computer Vision: Part VI, ECCV'10*, pages 337–350, Berlin, Heidelberg, 2010. Springer-Verlag.
- [11] R. Ng. *Digital Light Field Photography*. PhD thesis, Stanford, CA, USA, 2006. AAI3219345.
- [12] M. Potmesil and I. Chakravarty. Synthetic image generation with a lens and aperture camera model. *ACM Trans. Graph.*, 1(2):85–108, Apr. 1982.
- [13] N. Ratner and Y. Y. Schechner. Illumination multiplexing within fundamental limits. In *Computer Vision and Pattern Recognition, 2007. CVPR '07. IEEE Conference on*, pages 1–8, June 2007.
- [14] A. Veeraraghavan, R. Raskar, A. Agrawal, A. Mohan, and J. Tumblin. Dappled photography: Mask enhanced cameras

for heterodyned light fields and coded aperture refocusing. In *ACM SIGGRAPH 2007 Papers*, SIGGRAPH '07, New York, NY, USA, 2007. ACM.

- [15] J. Wu, C. Zheng, X. Hu, and F. Xu. Rendering realistic spectral bokeh due to lens stops and aberrations. *The Visual Computer*, 29(1):41–52, 2012.
- [16] C. Zhou and S. Nayar. What are good apertures for defocus deblurring? In *Computational Photography (ICCP), 2009 IEEE International Conference on*, pages 1–8, April 2009.